CHIN. PHYS. LETT. Vol. 38, No. 8 (2021) 086301 **Express Letter**

Superconductivity in Shear Strained Semiconductors

Chang Liu(刘畅)[1,2], Xianqi Song(宋贤齐)[1], Quan Li(李全)[1,2*], Yanming Ma(马琰铭)[1,2*], and Changfeng Chen(陈长风)[3*]

[1]*State Key Lab of Superhard Materials, and International Center for Computational Methods and Software, College of Physics, Jilin University, Changchun 130012, China*
[2]*International Center of Future Science, Jilin University, Changchun 130012, China*
[3]*Department of Physics and Astronomy, University of Nevada, Las Vegas, Nevada 89154, USA*

(Received 8 May 2021; accepted 25 June 2021; published online)

Semiconductivity and superconductivity are remarkable quantum phenomena that have immense impact on science and technology, and materials that can be tuned, usually by pressure or doping, to host both types of quantum states are of great fundamental and practical significance. Here we show by first-principles calculations a distinct route for tuning semiconductors into superconductors by diverse large-range elastic shear strains, as demonstrated in exemplary cases of silicon and silicon carbide. Analysis of strain driven evolution of bonding structure, electronic states, lattice vibration, and electron-phonon coupling unveils robust pervading deformation induced mechanisms auspicious for modulating semiconducting and superconducting states under versatile material conditions. This finding opens vast untapped structural configurations for rational exploration of tunable emergence and transition of these intricate quantum phenomena in a broad range of materials.

DOI: 10.1088/0256-307X/38/8/086301

Semiconductors and superconductors exhibit profound and distinct quantum phenomena. Materials that can host both behaviors offer an appealing platform for innovative research and development.[1] The quest to explore superconducting states in semiconductors has a long history dating back to 1960s.[2–7] Most works have taken two established routes: (i) external doping by atomic insertion or substitution or self-doping by alloying,[8] and (ii) application of high pressure.[9,10] The resulting electrically conducting states couple to another degree of freedom, e.g., lattice vibration (i.e., phonon), to generate superconductivity in chemically (doping) or physically (pressure) modulated semiconductors. In recent years, strain engineering has been employed to induce superconductivity at surfaces or thin films via adatom adsorption or interfacial lattice mismatch.[11–15] This approach is effective, but lacks flexibility of tuning the resulting superconducting states, since the strains are fixed once the surface or substrate conditions are set. It is desirable to explore further avenues for achieving more flexible and tunable modulation of semiconducting and superconducting states, preferably reversibly over large strain ranges and in ways that are compatible with nanoelectronic synthesis and characterization protocols.

Recent research revealed that diamond can be driven into a metallic state by biaxial compression-shear (CS) deformation, and charge redistribution and phonon softening at rising strains generate superconductivity in this ultralarge-bandgap insulator.[16] This surprising result suggests that shear-strain tuning may offer an effective tool for generating and tuning superconductivity in semiconductors. There are, however, crucial differences in structural and electronic properties distinguishing most semiconductors from diamond. In particular, diamond's unique tendency of graphitization accompanied by the associated large bonding changes plays a key role in inducing strong charge redistribution and phonon softening that drive superconductivity in its deformed crystal.[16] It is therefore compelling to probe how typical prominent semiconductors would deform under various shear strains and whether metallic and superconducting states would emerge, and if affirmative, how the driving mechanism would be related yet distinct compared to that in deformed diamond and, most crucially, whether these insights are generally applicable to wide-ranging semiconductors.

In this Letter, we report findings from first-principles calculations on emerging superconducting states in shear strained classic semiconductors Si and SiC. In contrast to diamond that develops superconductivity under special CS strains, Si and SiC host superconducting states under diverse shear conditions, including unconstrained pure shear strains, offering

Supported by the National Key Research and Development Program of China (Grant No. 2018YFA0703400), the National Natural Science Foundation of China (Grant Nos. 12074140 and 12034009), the China Postdoctoral Science Foundation (Grant No. 2020M681031), and the Program for JLU Science and Technology Innovative Research Team (JLUSTIRT).
*Corresponding authors. Email: liquan777@calypso.cn; mym@jlu.edu.cn; chen@physics.unlv.edu

expanded tunability for flexible and versatile experimental control and implementation. We analyze evolution of structural, electronic, phonon, and electron-phonon coupling with changing strains in elastically deformed Si and SiC and identify robust metallization and phonon softening mechanisms that should be applicable to a broad variety of materials. These findings showcase elastic shear-strain engineering as an effective tool for tuning semiconducting and superconducting states over large strain ranges, opening new access to hitherto little explored deformed material configurations for discovery of fascinating physics phenomena.

Silicon is known to undergo a series of structural transitions from the cubic diamond phase to β-tin, simple hexagonal (sh), and then hexagonal close packed (hcp) phases at increasing pressures,[17–19] and these high-pressure phases of Si are all metallic and superconducting with a peak T_c of 8.2 K reached at 15 GPa in the sh-Si phase.[20,21] The cubic diamond phase of Si can also host superconductivity under carrier doping via boron-atom insertion with $T_c \approx 0.35$ K,[22] which is an order of magnitude lower than that observed in boron doped diamond[23–25] due to much weaker bonding strength and lower phonon frequency in Si. Superconductivity has been induced in the cubic diamond phase of SiC by carrier doping through boron-atom insertion with $T_c \approx 1.4$ K.[26] There has been no report on pressure-induced superconductivity in the wide-bandgap semiconductor SiC. In this work, we show that full-range elastic shear-strain tuning offers an alternative and versatile means to produce and modulate superconductivity in Si and SiC, and that the obtained results suggest common and robust mechanisms for wide-ranging semiconductors.

For stress-strain calculations, we have employed VASP code[27] based on the density functional theory (DFT) in the local density approximation (LDA).[28,29] We have also calculated lattice dynamics and electron-phonon coupling (EPC) using the density-functional perturbation theory (DFPT) in linear response as implemented in QUANTUM ESPRESSO code.[30] Such calculations produce adequate structural and mechanical properties and describe well metallic states and produce fairly accurate T_c in metallized semiconductors, as extensively demonstrated in boron-doped diamond and silicon.[23,31–37] LDA calculations, however, are known to underestimate electronic bandgaps in semiconductors, so we have adopted the Heyd–Scuseria–Ernzerhof (HSE) hybrid functional[38,39] that accurately reproduces experimental bandgaps of Si and SiC.[40,41] More computational details are given in the Supplemental Material.[42]

From Eliashberg theory of superconductivity,[43,44] McMillan derived,[45] later modified by Allen and Dynes,[46] an analytic expression for transition temperature,

$$T_c = \frac{\omega_{\log}}{1.20}\exp\{-\frac{1.04(1+\lambda)}{\lambda-\mu^*(1+0.62\lambda)}\}, \qquad (1)$$

where $\omega_{\log}$ is a logarithmically averaged characteristic phonon frequency, and μ^* is the Coulomb pseudopotential which describes the effective electron-electron repulsion.[47] This equation is generally accurate for materials with EPC parameter $\lambda < 1.5$,[48–51] whereas a numerical solution to the Eliashberg equation[43] is more adequate at larger λ. The Coulomb pseudopotential μ^* is often treated as an adjustable parameter with values within a narrow range around 0.1 for most materials, making this formulism highly robust,[46–50] and compares well with the latest *ab initio* Eliashberg theory.[51] Smaller values of μ^* also occur, like $\mu^* = 0.06$ for a high-pressure phase of Si.[21] We choose 0.05 as a lower bound and 0.10 as a typical value for μ^* in this study. This ranged choice for μ^* is especially suitable here since the metallicity of the deformed semiconductors develops with rising strain, producing improved screening thus reduced μ^*, favoring the high end of predicted T_c values.

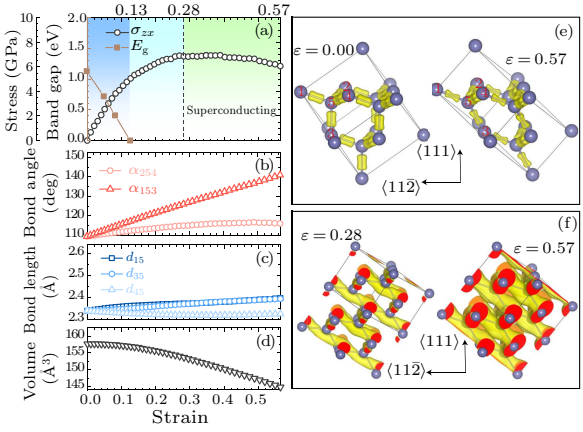

Fig. 1. (a) Stress and bandgap evolution of Si under the (111)[11$\bar{2}$] PS strain up to the dynamic stability limit $\epsilon = 0.57$. Metallization and superconducting states emerge at $\epsilon > 0.13$ and $\epsilon > 0.28$, respectively. Variations of (b) bond angle α_{153} between atom pairs 1–5 and 5–3 and α_{254} [see panel (e)], (c) three key bond lengths, d_{15}, d_{35} and d_{45}, and (d) the unit-cell volume. [(e), (f)] Structural snapshots with bonding and conducting charge density at selected strains.

To explore emerging metallic and superconducting states in deformed Si crystal, we have examined its structural and stress responses under various shear strains, which are highly effective deformation modes in generating large-range creep-like flat stress-strain curves that are indicative of metallization of covalent crystals under large strains.[52] We have identified multiple shear strain paths showing flattened stress curves with promising tendency for metalliza-

tion (Fig. S1, Ref. [42]). Here we focus primarily on the (111)[11$\bar{2}$] pure shear (PS) mode as an exemplary case with a pronounced creep-like stress response. Results in Fig. 1(a) show that stress initially rises quickly with increasing shear strain to $\epsilon \approx 0.13$, where deformed Si becomes metallic (see below), then the rate of stress increase tapers off considerably as the degree of metallicity progressively develops, and the curve becomes nearly flat at $\epsilon \approx 0.25$ and remains so over an extended range of further rising strain up to the dynamic stability limit $\epsilon \approx 0.57$, beyond which imaginary phonon modes develop. This extraordinarily extended range of elastic deformation opens up vast untapped material configurations for exploring novel phenomena like reversibly tunable metallicity and superconductivity in Si, and this approach may prove generally effective for producing similar phenomena in other semiconductors.

The electronic properties of Si are highly sensitive to changes in its bonding environment. Metallic states appear in Si upon a large variety of small to moderate deformations once the Si crystal deviates from its native cubic diamond phase well before reaching the β-tin phase.[53,54] Calculated results show that the electronic bandgap E_g of Si drops quickly along the (111)[11$\bar{2}$] PS strain path, leading to a full closure at $\epsilon = 0.13$ [Fig. 1(a)]. The electronic density of states (EDOS) at the Fermi level, $N(E_F)$, rises steadily with increasing strain, enhancing the metallicity of progressively deformed Si under various loading conditions (see Table 1).

The concurrence of significant lattice softening, as indicated by the flattening stress curve, and emerging metallicity, as signified by the bandgap closure (Fig. S2, Ref. [42]) and rising $N(E_F)$ under the (111)[11$\bar{2}$] shear strains in Si is dominated by an unusually large angular expansion mode with small bond elongations [Figs. 1(b) and 1(c)], thereby sustaining significant redistribution of bonding charge without bond breaking, reminiscent of the situation in CS deformed diamond.[52] However, in sharp contrast to the volume expanding tendency in diamond and related strong covalent solids,[55–59] Si crystal undergoes a monotonic volume contraction up to dynamic stability limit at $\epsilon = 0.57$ [Fig. 1(d)], which stems from a large reduction of the distance between the (001) planes under the large angular deformation mode in the Si crystal (Fig. S3, Ref. [42]). We find fairly uniform bonding charge density on both the original undeformed bonds and elongated and partially charge depleted bonds at large strains [Fig. 1(e)]. Emerging conducting charges stemming from the depleted bonding charges are assessed by integrating the electronic states over a small (0.3 eV) energy window below the Fermi level; the results [Fig. 1(f)] show that these conducting charges form a well separated layered pattern as superconductivity emerges (at $\epsilon = 0.28$), but a three-dimensional pattern develops at larger strains (e.g., at $\epsilon = 0.57$), suggesting a crossover in transport behaviors in increasingly strained and metallic Si crystal.

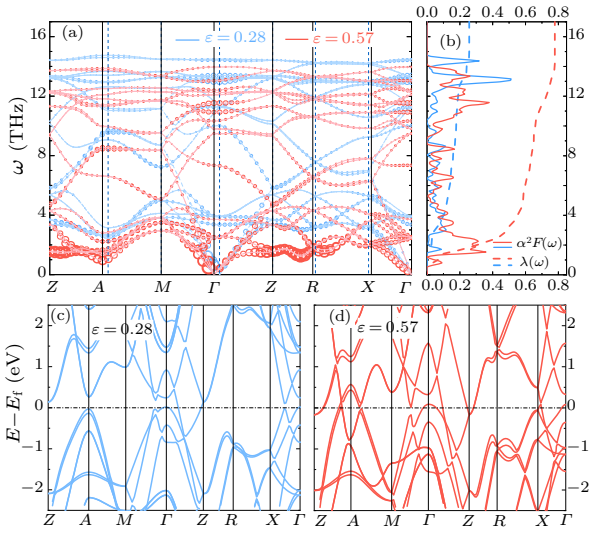

Fig. 2. (a) Phonon dispersions at selected (111) [11$\bar{2}$] PS strains with the strength of q-resolved λ_q indicated by circle size. The solid and dashed vertical lines indicate [also in Figs. 3(b), 3(e) and 4(b)] the positions of the high-symmetry points in the reciprocal lattice at different indicated shear strains. (b) Spectral function $\alpha^2F(\omega)$ and $\lambda(\omega)$. [(c), (d)] Calculated electronic band structures at $\epsilon = 0.28$ and $\epsilon = 0.57$, respectively.

Figure 2 shows phonon dispersion and spectral function $\alpha^2F(\omega)$ and EPC parameter $\lambda(\omega) = 2\int_0^\omega \frac{\alpha^2F(\omega)}{\omega}d\omega$ at selected (111)[11$\bar{2}$] PS strains. At $\epsilon = 0.28$ where superconducting states start to emerge, EPC is contributed by a broad range of low- and high-frequency phonon modes, but at large strains (e.g., $\epsilon = 0.57$) EPC is dominated by greatly softened low-frequency modes. The nearly uniform distribution of EPC throughout the Brillouin zone is in stark contrast to CS deformed diamond where EPC is highly anisotropic and concentrated at the lattice vibrations associated with the most charge-depletion softened bonds.[16] In shear deformed Si, bonds are more uniformly stretched [Fig. 1(e)] with even charge distribution, leading to pronounced and nearly uniform phonon softening and EPC enhancement. It is noted that the phonon softening is intimately related to the flattening of the stress curves (Fig. S4, Ref. [42]), both stemming from the strain weakened bonding structures. Also shown in Fig. 2 are the electronic band structures at the selected shear strains, and it is seen that increasing strain leads to more extensive band crossing at the Fermi level, which would significantly impact electronic transport behaviors.

To test robustness of superconductivity in shear strained Si, we have examined the results under the (11$\bar{2}$)[111] CS and (111)[11$\bar{2}$] tension shear (TS) (Fig. S5, Ref. [42]). The results in Fig. 3 (see Fig. S6,

Ref. [42], for electronic band structures at the selected strains) show the same patterns of flattened stress curves, quick bandgap reduction and closure, and ensuing emergence of superconducting states, although the rise of T_c is limited by shortened dynamic stability range compared to the PS case. There is clear dominance by low-frequency modes on the phonon softening and EPC enhancement, demonstrating that the same robust mechanism is driving superconductivity in all these differently deformed Si lattices. These results establish consistent trends in diverse shear-strain enhanced $N(E_F)$, softened ω_{log}, and higher λ and T_c (see Table 1).

Table 1. Computed $N(E_F)$ (states·spin^{-1}·Ry^{-1}·cell^{-1}), ω_{log} (K), λ and T_c (K) for Si and SiC at various PS, CS or TS strains. Two T_c values set the range for $\mu^* = 0.10$ and 0.05.

	Strain	$N(E_F)$	ω_{log}	λ	T_c
Si PS (111)[11$\bar{2}$]	0.28	9.7	282	0.26	0.0–0.4
Si PS (111)[11$\bar{2}$]	0.42	13.3	219	0.42	1.3–2.9
Si PS (111)[11$\bar{2}$]	0.53	15.8	157	0.67	4.8–7.2
Si PS (111)[11$\bar{2}$]	0.57	16.6	145	0.78	6.5–8.7
Si CS (11$\bar{2}$)[111]	0.22	9.5	260	0.26	0.0–0.3
Si CS (11$\bar{2}$)[111]	0.27	11.0	218	0.35	0.3–1.4
Si CS (11$\bar{2}$)[111]	0.36	12.3	153	0.50	1.8–3.5
Si TS (111)[11$\bar{2}$]	0.28	11.0	261	0.33	0.3–1.2
Si TS (111)[11$\bar{2}$]	0.39	14.6	207	0.51	2.8–5.1
SiC PS (111)[11$\bar{2}$]	0.49	5.3	628	0.22	0.0–0.2
SiC PS (111)[11$\bar{2}$]	0.68	6.4	393	0.38	1.3–3.7

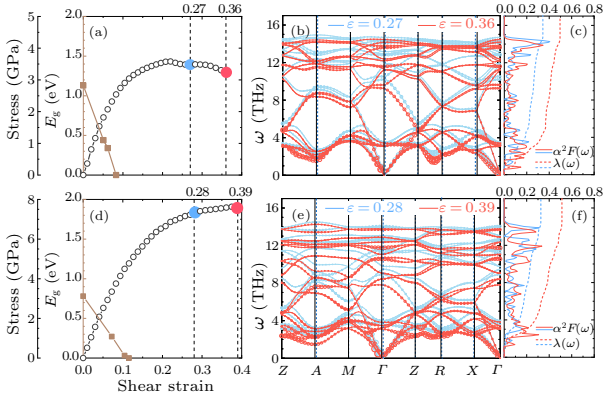

Fig. 3. [(a), (d)] Stress and bandgap evolution of Si under (11$\bar{2}$)[111] CS or (111)[11$\bar{2}$] TS strains. [(b), (e)] Phonon dispersions at selected strains with the strength of q-resolved λ_q indicated by circle size. [(c), (f)] Spectral functions $\alpha^2F(\omega)$ and $\lambda(\omega)$.

We now turn to SiC, which comprises a C–Si bonding network in diamond structure and a much larger band gap compared to Si.[42] We examine the (111)[11$\bar{2}$] PS that has the most flattened stress curve among the examined cases.[42] Compared to Si, the bandgap of SiC decreases with rising strain at a slightly reduced but still fast rate, and the metallic then superconducting states develop quickly as indicated in Fig. 4(a), which reinforces the notion that Si and SiC share key structural and electronic response patterns under shear loading conditions, raising excellent prospects that these behaviors are commonly present in shear-strained semiconductors. Interestingly, calculated results in Fig. 4(b) show that EPC in shear deformed SiC is mainly contributed by phonon modes across a broad frequency range but concentrated in momentum space near the Γ and A points, which is similar to the situation in CS deformed diamond[16] but different from the nearly uniform distributions in Si under diverse PS, CS, or TS strains [see results in Figs. 2(a), 3(b) and 3(e)]. Despite such different EPC characteristics, Si and SiC share the most prominent features of shear-strain induced robust metallization and strong phonon softening, leading to substantial superconducting states in distinct material environments. Such diversity bodes well for finding similar phenomena driven by the same general mechanisms in many other semiconductors.

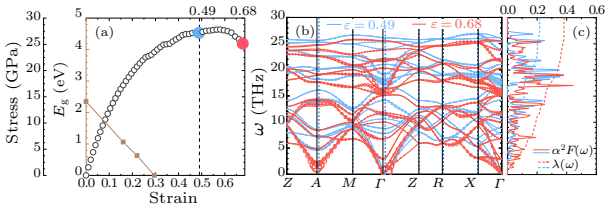

Fig. 4. (a) Stress and bandgap evolution of SiC under (111)[11$\bar{2}$] PS strains. (b) Phonon dispersions at selected strains with the strength of q-resolved λ_q indicated by circle size. (c) Spectral function $\alpha^2F(\omega)$ and $\lambda(\omega)$.

Carrier doping has produced superconductivity with T_c of 0.35 K in Si[22] and 1.4 K in SiC.[26] Here, we show that diverse shear strains can effectively modulate T_c over extended ranges up to much higher values of 8.7 K for Si and 3.7 K for SiC. These results underscore excellent prospects for inducing vigorous superconducting states in elastically deformed semiconductors. These superior T_c values under tunable shear strains are well above those achieved in semiconducting or conducting films under fixed tensile strains by lattice mismatch,[11–14] making shear-strain tuning a desirable approach.

High pressure can effectively modulate material properties,[60–62] but stringent equipment requirements impose a very high barrier for most practical implementation; in contrast, strain tuning is compatible with advanced material characterization protocols, and avoids the need for external carriers, usually by ion implantation that commonly causes structural and charge disorder with uncontrolled complications in the host material.[1,8] Tuning superconductivity in elastically deformed semiconductors allows for substantial property modulations, as seen in a recent experiment showing that soft phonon modes associated with unique bond contractions induced by interfacial strains induced surprising superconductivity in RuO_2 films.[14] Such coherent epitaxy is the current

state of the art in strain engineering.[11−14] The latest nanoscale fabrication and imaging techniques have demonstrated reversible ultralarge elastic deformation approaching the theoretical limits under diverse loading conditions.[63−67] These powerful techniques open up vast structural configuration space for exploring richer material behaviors and physics processes beyond the traditional paradigm of structural stability at quasi-hydrostatic pressures to discover novel material behaviors and enable new functionalities with major technological impact.

In summary, we have uncovered via first-principles calculations robust superconducting states in shear strained Si and SiC crystals under diverse loading conditions. Analysis of structural, electronic, phonon, and electron-phonon coupling behaviors under evolving strains reveals consistent patterns and trends of shear deformation induced and enhanced metallization and phonon softening, resulting in vigorous superconducting states that host rising T_c at progressively increasing strains. This work opens a promising avenue for inducing and tuning superconducting states in semiconductors by versatile shear strains. The key physics processes and mechanisms unveiled here are insensitive to material details and, therefore, are expected to be general phenomena not limited to Si and SiC or cubic crystals, and should remain robust and applicable to wide-ranging semiconductors. While covalent crystals provide a favorable platform for the physics described here, because of their highly concentrated and directional bonding structures, we expect that strain induced charge redistribution and phonon softening provide an effective approach for tuning superconductivity in a broad variety of materials. Advanced nanoscale synthesis and characterization techniques have produced high-quality specimens and tested mechanical properties,[63−68] and these techniques are also well equipped to operate at cryogenic conditions for versatile physical property measurements at extremely low temperatures,[69−71] making experimental verification of our predicted results feasible.

The present findings have major implications beyond tuning superconducting states in semiconductors, e.g., for deciphering exceptional phonon-mediated superconductors like the long-sought metallic hydrogen[72,73] and recently discovered superhydrides,[74−77] which have been predicted or demonstrated to superconduct near room temperature at megabar pressures. Non-hydrostatic conditions like uniaxial compression and shear strains are inevitably present in such extreme environments, e.g., transport studies employing diamond anvil cell with solid or even no pressure transmitting mediumexerting major influence on material behaviors, such as incipient structural instability that has been postulated to impact superconductivity in LaH_{10}.[78] Current experimental methods employing traditional or rotational diamond anvil cell setups are capable of producing large shear-strain conditions at high pressures, and recent studies using these setups have revealed significant shear-induced property modulations such as altered kinetics of pressure induced graphite-to-diamond transition[79] and discovery of a new shear-driven formation route for diamond.[80] Such capabilities provide a powerful technique for probing shear strain effects on diverse phonon-mediated superconductors, e.g., high-T_c superhydrides. This study provides a strong impetus for exploring effects of broadly defined strains on modulating these fascinating superconducting materials. Work along this line may prove fruitful in discovering intriguing phenomena and elucidating key mechanisms.

Reported calculations utilized computing facilities at the High-Performance Computing Center of Jilin University and Tianhe2-JK at the Beijing Computational Science Research Center.

References

[1] Blase X, Bustarret E, Chapelier C, Klein T and Marcenat C 2009 *Nat. Mater.* **8** 375
[2] Gurevich V L, Larkin A I and Firsov Y A 1962 *Sov. Phys. Solid State* **4** 131
[3] Cohen M L 1964 *Phys. Rev.* **134** A511
[4] Cohen M L 1964 *Rev. Mod. Phys.* **36** 240
[5] Schooley J F, Hosler W R and Cohen M L 1964 *Phys. Rev. Lett.* **12** 474
[6] Schooley J F, Hosler W R, Ambler E, Becker J H, Cohen M L and Koonce C S 1965 *Phys. Rev. Lett.* **14** 305
[7] Hein R A, Gibson J W, Mazelsky R, Miller R C and Hulm J K 1964 *Phys. Rev. Lett.* **12** 320
[8] Bustarret E 2015 *Physica C* **514** 36
[9] Mao H K, Chen X J, Ding Y, Li B and Wang L 2018 *Rev. Mod. Phys.* **90** 015007
[10] Liu Z, Dong Q, Shan P, Wang Y, Dai J, Jana R, Chen K, Sun J, Wang B, Yu X, Liu G, Uwatoko Y, Sui Y, Yang H, Chen G and Cheng J 2020 *Chin. Phys. Lett.* **37** 047102
[11] Hicks C W, Brodsky D O, Yelland E A, Gibbs A S, Bruin J A N, Barber M E, Edkins S D, Nishimura K, Yonezawa S, Maeno Y, Mackenzie A P 2014 *Science* **344** 283
[12] Ahadi K, Galletti L, Li Y, Salmani-Rezaie S, Wu W and Stemmer S 2019 *Sci. Adv.* **5** eaaw0120
[13] Wu X, Ming F, Smith T S, Liu G, Ye F, Wang K, Johnston S and Weitering H H 2020 *Phys. Rev. Lett.* **125** 117001
[14] Uchida M, Nomoto T, Musashi M, Arita R and Kawasaki M 2020 *Phys. Rev. Lett.* **125** 147001
[15] Yuan Y H, Wang X T, Song C L, Wang L L, He K, Ma X C, Yao H, Li W and Xue Q K 2020 *Chin. Phys. Lett.* **37** 017402
[16] Liu C, Song X, Li Q, Ma Y M and Chen C F 2020 *Phys. Rev. Lett.* **124** 147001
[17] Chang K J and Cohen M L 1984 *Phys. Rev. B* **30** 5376
[18] Olijnyk H, Sikka S K and Holzapfel W B 1984 *Phys. Lett. A* **103** 137
[19] Hu J Z and Spain I L 1984 *Solid State Commun.* **51** 263
[20] Mignot J M, Chouteau G and Martinez G 1985 *Physica B* **135** 235
[21] Chang K J, Dacorogna M M, Cohen M L, Mignot J M, Chouteau G and Martinez G 1985 *Phys. Rev. Lett.* **54** 2375

[22] Bustarret E, Marcenat C, Achatz P, Kacmarcik J, Levy F, Huxley A, Ortega L, Bourgeois E, Blase X, Debarre D and Boulmer J 2006 *Nature* **444** 465
[23] Ekimov E A, Sidorov V A, Bauer E D, Melnik N N, Curro N J, Thompson J D and Stishov S M 2004 *Nature* **428** 542
[24] Takano Y, Nagao M, Sakaguchi I, Tachiki M, Hatano T, Kobayashi K, Umezawa H and Kawarada H 2004 *Appl. Phys. Lett.* **85** 2851
[25] Zhang G, Turner S, Ekimov E A, Vanacken J, Timmermans M, Samuely T, Sidorov V A, Stishov S M, Lu Y, Deloof B, Goderis B, Van Tendeloo G, Van de Vondel J and Moshchalkov V V 2014 *Adv. Mater.* **26** 2034
[26] Ren Z A, Kato J, Muranaka T, Akimitsub J, Kriener M and Maeno Y 2007 *J. Phys. Soc. Jpn.* **76** 103710
[27] Kresse G and Furthmüller L 1996 *Phys. Rev. B* **54** 11169
[28] Perdew J P and Zunger A 1981 *Phys. Rev. B* **23** 5048
[29] Ceperley D M and Alder B J 1980 *Phys. Rev. Lett.* **45** 566
[30] Giannozzi P *et al.* 2009 *J. Phys.: Condens. Matter* **21** 395502
[31] Boeri L, Kortus J and Andersen O K 2004 *Phys. Rev. Lett.* **93** 237002
[32] Lee K W and Pickett W E 2004 *Phys. Rev. Lett.* **93** 237003
[33] Xiang H J, Li Z Y, Yang J L, Hou J G and Zhu Q S 2004 *Phys. Rev. B* **70** 212504
[34] Blase X, Adessi C and Connetable D 2004 *Phys. Rev. Lett.* **93** 237004
[35] Ma Y, Tse J S, Cui T, Klug D D, Zhang L, Xie Y, Niu Y and Zou G 2005 *Phys. Rev. B* **72** 014306
[36] Giustino F, Yates J R, Souza I, Cohen M L and Louie S G 2007 *Phys. Rev. Lett.* **98** 047005
[37] Noffsinger J, Giustino F, Louie S G and Cohen M L 2009 *Phys. Rev. B* **79** 104511
[38] Heyd J, Scuseria G E and Ernzerhof M 2003 *J. Chem. Phys.* **118** 8207
[39] Heyd J, Scuseria G E and Ernzerhof M 2006 *Erratum: J. Chem. Phys.* **124** 219906
[40] Bludau W, Onton A and Heinke W 1974 *J. Appl. Phys.* **45** 1846
[41] Hunphreys R G, Bimberg D and Choyke W J 1981 *Solid State Commun.* **39** 163
[42] The Supplemental Material provides further details on computational procedures and parameters, stress-strain relations under various loading conditions for Si and SiC, electronic density of states calculated using the HSE functional to determine the band gap of Si and SiC under various shear strains, structural changes of shear strained Si, relation between the flattening of the stress curve and phonon frequency softening for Si and electronic band structures at selected shear strains for Si and SiC.
[43] Eliashberg G M 1960 *Sov. Phys. JETP* **11** 696
[44] Scalapino D J, Schrieffer J R and Wilkins J W 1966 *Phys. Rev.* **148** 263
[45] McMillan W L 1968 *Phys. Rev.* **167** 331
[46] Allen P B and Dynes R C 1975 *Phys. Rev. B* **12** 905
[47] Morel P and Anderson P W 1962 *Phys. Rev.* **125** 1263
[48] McMillan W L and Rowell J M 1969 *Superconductivity* edited by Parks R D (New York: Marcel Dekker) vol 1 p 561
[49] Carbotte J P 1990 *Rev. Mod. Phys.* **62** 1027
[50] Carbotte J P and Marsiglio F 2003 *Electron-Phonon Superconductivity* in *The Physics of Superconductors* edited by Bennemann K H and Ketterson J B (Berlin: Heidelberg)
[51] Sanna A, Flores-Livas J A, Davydov A, Profeta G, Dewhurst K, Sharma1 S and Gross E K U 2018 *J. Phys. Soc. Japn.* **87** 041012
[52] Liu C, Song X, Li Q, Ma Y M and Chen C F 2019 *Phys. Rev. Lett.* **123** 195504
[53] Shen G, Ikuta D, Sinogeikin S, Li Q, Zhang Y and Chen C F 2012 *Phys. Rev. Lett.* **109** 205503
[54] Zarkevich N A, Chen H, Levitas V I and Johnson D D 2018 *Phys. Rev. Lett.* **121** 165701
[55] Zhang Y, Sun H and Chen C F 2005 *Phys. Rev. Lett.* **94** 145505
[56] Zhang Y, Sun H and Chen C F 2006 *Phys. Rev. B* **73** 144115
[57] Zhang Y, Sun H and Chen C F 2006 *Phys. Rev. B* **73** 064109
[58] Li B, Sun H and Chen C F 2014 *Nat. Commun.* **5** 4965
[59] Li B, Sun H and Chen C F 2016 *Phys. Rev. Lett.* **117** 116103
[60] Chen X, Zhan X H, Wang X J, Deng J, Liu X B, Chen X, Guo J G and Chen X L 2021 *Chin. Phys. Lett.* **38** 057402
[61] Gu Q Y, Xing D Y and Sun J 2019 *Chin. Phys. Lett.* **36** 097401
[62] Zhang X, Luo T C, Hu X Y, Guo J, Lin G C, Li Y H, Liu Y Z, Li X K, Ge J, Xing Y, Zhu Z W, Gao P, Sun L L and Wang J 2019 *Chin. Phys. Lett.* **36** 057402
[63] Zhang H, Tersoff J, Chen S X H, Zhang Q, Zhang K, Yang Y, Lee C S, Tu K N, Li J and Lu Y 2016 *Sci. Adv.* **2** e1501382
[64] Banerjee A, Bernoulli D, Yuen H Z M F, Liu J, Dong J, Ding F, Lu J, Dao M, Zhang W, Lu Y and Suresh S 2018 *Science* **360** 300
[65] Nie A, Bu Y, Li P, Zhang Y, Jin T, Liu J, Su Z, Wang Y, He J, Liu Z, Wang H, Tian Y and Yang W 2019 *Nat. Commun.* **10** 5533
[66] Chen M, Pethö L, Sologubenko A S, Ma H, Michler J, Spolenak R and Wheeler J M 2020 *Nat. Commun.* **11** 2681
[67] Shi Z, Dao M, Tsymbalov E, Shapeev A, Li J and Suresh S 2020 *Proc. Natl. Acad. Sci. USA* **117** 24634
[68] Dang C, Chou J, Dai B, Chou C, Yang Y, Fan R, Lin W, Meng F, Hu A, Zhu J, Han J, Minor A M, Li J and Lu Y 2021 *Science* **371** 76
[69] Luo W, Boselli M, Poumirol J, Ardizzone I, Teyssier J, van der Marel D, Gariglio S, Triscone J and Kuzmenko A B 2019 *Nat. Commun.* **10** 2774
[70] Jiang S, Xie H, Shan J and Mak K F 2020 *Nat. Mater.* **19** 1295
[71] Tang Y, Li L, Li T, Xu Y, Liu S, Barmak K, Watanabe K, Taniguchi T, MacDonald A H, Shan J and Mak K F 2020 *Nature* **579** 353
[72] Ashcroft N W 1968 *Phys. Rev. Lett.* **21** 1748
[73] McMahon J M and Ceperley D M 2011 *Phys. Rev. B* **84** 144515
[74] Sun Y, Lv J, Xie Y, Liu H and Ma Y M 2019 *Phys. Rev. Lett.* **123** 097001
[75] Drozdov A P, Kong P P, Minkov V S, Besedin S P, Kuzovnikov M A, Mozaffari S, Balicas L, Balakirev F F, Graf D E, Prakapenka V B, Greenberg E, Knyazev D A, Tkacz M and Eremets M I 2019 *Nature* **569** 528
[76] Somayazulu M, Ahart M, Mishra A K, Geballe Z M, Baldini M, Meng Y, Struzhkin V V and Hemley R J 2019 *Phys. Rev. Lett.* **122** 027001
[77] Hong F, Yang L X, Shan P F, Yang P T, Liu Z Y, Sun J P, Yin Y Y, Yu X H, Cheng J G and Zhao Z X 2020 *Chin. Phys. Lett.* **37** 107401
[78] Sun D, Minkov V S, Mozaffari S, Chariton S, Prakapenka V B, Eremets M I, Balicas L and Balakirev F F 2020 arXiv:2010.00160 [cond-mat.supr-con]
[79] Gao Y, Ma Y Z, An Q, Levitas V, Zhang Y, Feng B, Chaudhuri J and Goddard W A 2019 *Carbon* **146** 364
[80] Dong J, Yao Z, Yao M, Li R, Hu K, Zhu L, Wang Y, Sun H, Sundqvist B, Yang K and Liu B 2020 *Phys. Rev. Lett.* **124** 065701

Supplemental Material for "Superconductivity in Shear Strained Semiconductors"

Chang Liu(刘畅),[1,2] Xianqi Song(宋贤齐),[1] Quan Li (李全),[1,2,*]
Yanming Ma(马琰铭),[1,2,†] and Changfeng Chen(陈长风)[3,‡]

[1]*International Center for Computational Methods & Software, State Key Lab of Superhard Materials, College of Physics, Jilin University, Changchun 130012, China*
[2]*International Center of Future Science, Jilin University, Changchun 130012, China*
[3]*Department of Physics and Astronomy, University of Nevada, Las Vegas, Nevada 89154, USA*

Here we provide a systematic description of details on computational methods used in the present work and additional details supporting several results presented in the main text.

DETAILS ON COMPUTATIONAL METHODS

The first-principles energetic calculations and stress-strain relations reported in this work have been carried out using the VASP code [1], adopting the projector augmented wave (PAW) approach [2] with the valence electron configuration of s^2p^2 for both silicon and carbon, which are each described by an eight-atom unit cell. The local density approximation (LDA) has been used to describe the exchange and correlation potential between electrons as parametrized by the Ceperley and Alder functional [3]. An energy cutoff of 500 eV for Si and 800 eV for SiC and a Monkhorst-Pack grid [4] with a maximum spacing of 0.18 $Å^{-1}$ are adopted, achieving an energy convergence around 1 meV per atom with residual forces and stresses less than 0.005 eV$Å^{-1}$ and 0.1 GPa, respectively. Electronic band gaps are determined by calculations using the hybrid functional of Heyd-Scuseria-Ernzerhof (HSE) [5, 6], and the resulted band gaps for Si and SiC are 1.13 eV and 2.35 eV, respectively, which are in excellent agreement with experimental data [7, 8]. On this basis, the HSE band gaps for the deformed Si and SiC crystals are expected to provide a good description for strain induced band-gap modulations, especially the band-gap closure that signals the onset of metallization in each case.

Stress-strain relations under diverse loading conditions are calculated under a biaxial stress state that contains a shear stress and a normal compressive or tensile stress component. This approach covers the pure shear case in the limit of zero normal stress and simulates a rich variety of loading environments containing various biaxial stress states [9–11]. The shape of the deformed unit cell and atomic relaxation are determined completely at each step by the constrained structural optimization. The starting position for each strain step is taken from the relaxed coordinates of the previous strain step to ensure the quasistatic strain path, with a strain increment of 0.01 in each of the first five steps, which are in mostly linear elastic range, and then 0.005 for each subsequent steps. At each step, the applied shear strain is fixed to determine the shear stress σ_{xz}, while the other five independent components of the strain tensors and all the atoms inside the unit cell are simultaneously relaxed until the normal stress component (σ_{zz}) reaches a specified value, namely $\sigma_{zz} = \sigma_{xz}\tan\phi$ or $\sigma_{zz} = c$, where ϕ is an angular variable to adjust the ratio of the normal and shear components of the biaxial stress and c is a constant normal compressive or tensile stress. Meanwhile, all other four components of the Hellmann-Feynman stress tensor and the force on each atom become negligibly small after the full relaxation, typically less than 0.1 GPa and 0.005 eV·$Å^{-1}$, respectively. In this work, we have examined Si under diverse shear strains, including pure shear (PS), variable constrained shear (CS) with ϕ=68° corresponding to the prominent Vickers shear stress state [9–11], and constant tensile shear (TS) with c = 10 GPa, and SiC under PS stress condition.

Lattice dynamics and electron-phonon coupling behaviors have been calculated using the density-functional perturbation theory (DFPT) in linear response as implemented in the Quantum Expresso code [12], adopting a kinetic energy cutoff of 40 Ry and 70 Ry for Si and SiC, respectively. A k-mesh of 16×16×24 was used for the electronic calculations and a 4×4×6 q-mesh for the lattice dynamics calculations to achieve good convergence. Dynamic stability of deformed crystals was determined by checking for the absence of imaginary phonon modes, and the electron-phonon coupling (EPC) behaviors were evaluated and superconductivity assessed up to the highest strain for the dynamically stable structure on each chosen deformation path.

Phonon calculations in this work are performed without considering anharmonic effects. The stress-strain curves are determined by quasistatic structural optimization following the standard procedure, where stress is calculated by taking the derivative of the energy of the strained crystal with respect to strain. Phonon calculations within the harmonic approximation are subsequently performed to check the dynamic stability along specific deformation paths. Anharmonic effects could influence the dynamic stability of the deformed structure, thus affect the stable strain range of the stress-strain curve. It is noted, however, that anharmonicity is appreciable at high temperatures [13]. In this work, the superconducting states of deformed Si and SiC emerge at very low temperatures (below 10 K) and, therefore, no significant anharmonicity is expected. Moreover, re-

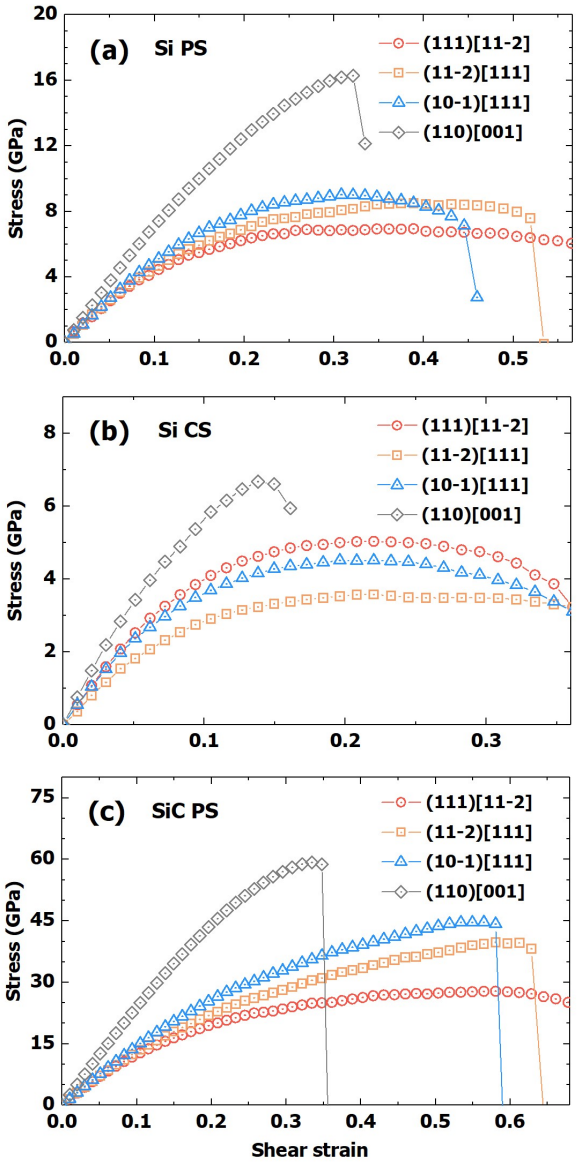

FIG. S1: Stress response under various shear-strain conditions. (a) Si under pure shear (PS), (b) Si under constrained shear (CS) and (c) SiC under PS strains. Specific shear slip directions are listed in each panel, and the most flattened curves, i.e., Si PS (111)[11-2], Si CS (11-2)[111] and SiC PS (111)[11-2], which represent the most favorable cases for metallization, are selected as shown in the main text. Covalent solids like diamond and Si host strongly directional bonding configurations, generating highly anisotropic stress responses. In this work, our goal is to explore strain-induced metallic and superconducting structure in Si; we therefore have mostly focused on stress responses along the (111)[11-2] PS and several closely related deformation paths. For comparison, we also show the shear-strain curve under the (110)[001] PS strain that exhibits a steeper rise of stress, which is commonly seen in covalent solids.

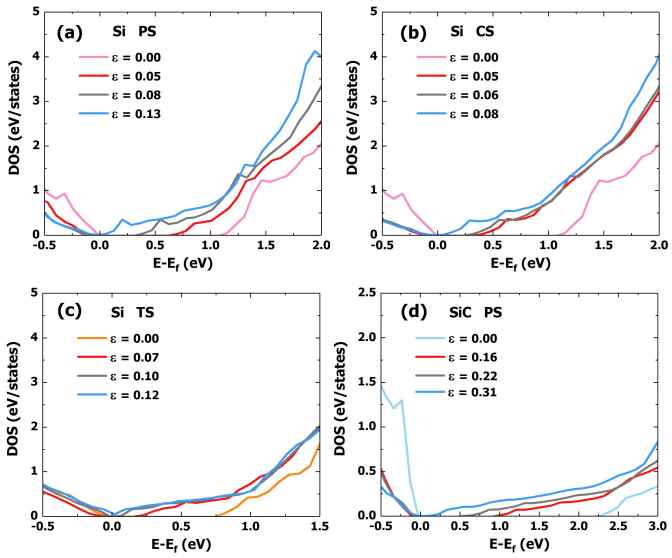

FIG. S2: Electronic band gap from HSE calculations under various shear-strain conditions. (a) Si PS (111)[11-2], (b) Si CS (11-2)[111], (c) Si TS (111)[11-2], (d) SiC PS (111)[11-2]. Results at selected strain points are shown.

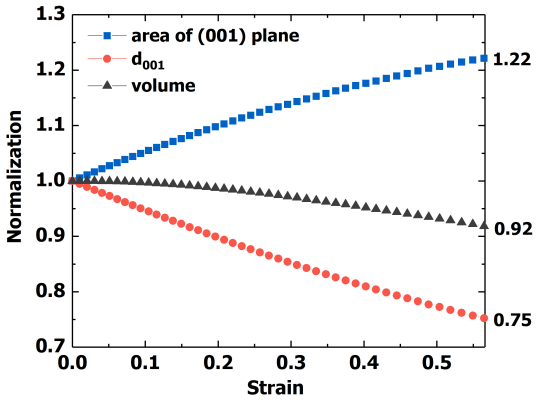

FIG. S3: The evolution of normalized (to the values of the unstrained crystal) lattice spacing between the (001) planes (d_{001}), the unit-cell area of the (001) plane and the unit-cell volume of Si under the (111)[11-2] PS strains. In the tetrahedrally bonded environment of Si crystal lattice, each Si atom has a large void site aligned opposite to one of its nearest-neighbor atoms [22]. The void positions and Si atom positions can be viewed as two face-center-cubic sublattices in the crystal structure. Under large deformations, such as the (111)[11-2] PS strains, a large angular expansion mode along with relatively small bond elongations causes a prominent contraction of the lattice spacing between the (001) planes, which is steeper than the expansion of the area of the (001) planes, leading to the reduced volume of the void, and thus an overall reduction of volume for the deformed crystal.

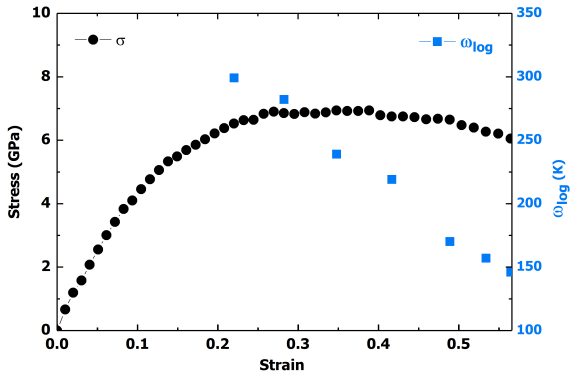

FIG. S4: Calculated logarithmic average phonon frequencies as a function of strain for Si under the (111)[11-2] PS deformation mode. There is a clear relation between the flattening of the stress-strain curve, which reflects the weakening of the bonding interaction in the deformed crystal, and a sharp and steady decline of the logarithmic average phonon frequencies in the (super)conducting phase of Si.

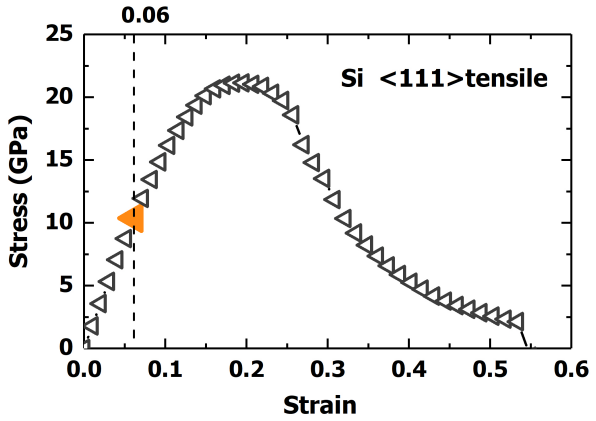

FIG. S5: Stress response of Si under (111) tensile strain. A point at 6% strain with a stress of 10 GPa near the middle of the elastic range, is selected as a representative condition for the evaluation of Si under the TS (111)[11-2] strains.

cent study shows that Si and diamond have the lowest degree of anharmonicity among all the crystals [14]. SiC involves the same two elements in the same crystal structure and is therefore expected to possess a similarly low level of degree of anharmonicity. Further, recent experiments demonstrated that nearly defect-free silicon and diamond nanostructures can approach theoretical strain and stress limits [15–20]. These studies show that achieving theoretically predicted large structural deformation is feasible. Overall, we expect that anharmonic effects will not have any appreciable impact on the main conclusions of our reported work.

Previous research revealed that anharmonic effect

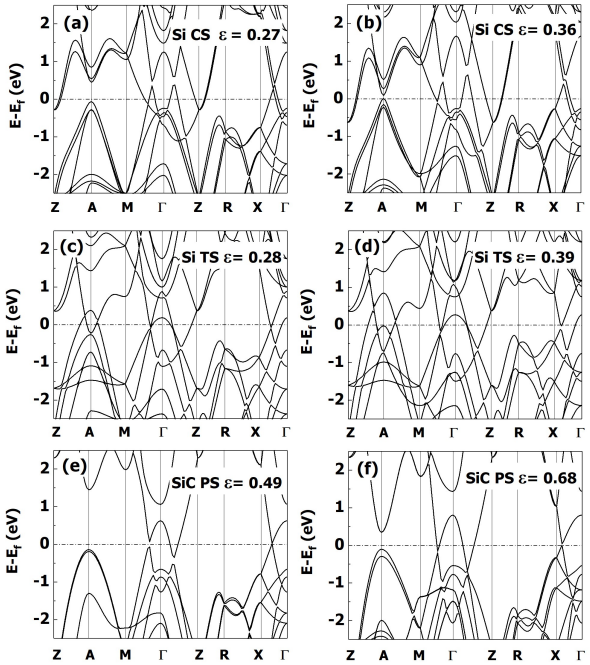

FIG. S6: Electronic band structures of (a, b) Si under the (11-2)[111] CS strains, (c, d) Si under the (111)[11-2] TS strains, and (e, f) SiC under the (111)[11-2] PS strains. These results show clear trends of shear strain driven increase of band crossing at the Fermi level, similar to the results for Si under the (111)[11-2] PS strains shown in Figs. 2(c) and 2(d).

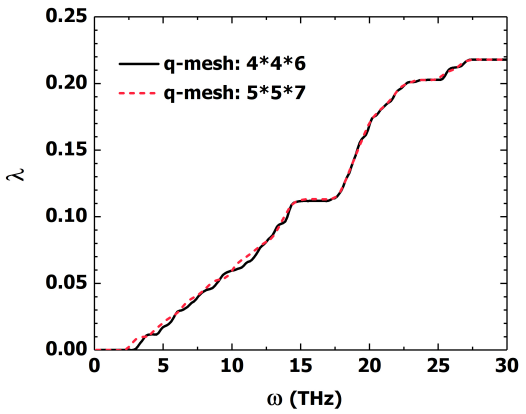

FIG. S7: Mesh convergence test for the calculated coupling integral $\lambda(\omega)$ at selected PS strain of 0.49 in deformed SiC. An 8-atoms cell is used in the calculations for electron-phonon coupling parameter. The calculated coupling integral $\lambda(\omega)$ at ϵ=0.49 with 4×4×6 and 5×5×7 q mesh generates 34 and 54 irreducible q points, respectively. The calculations with the distinct q-mesh choices yield nearly identical integrated λ values and Tc values, confirming that the q-mesh of 4×4×6 used in the present work is adequate to provide a reliable description for the phonon-mediated superconductivity.

could eliminate imaginary phonon modes and stabilize crystal structure that is dynamically unstable according to phonon calculations under harmonic approximation [21]. Such effects could impact structural stability of crystals under large strains, possibly leading to increased strain range and enhanced physical properties such as metallicity and superconductivity, especially in materials that host large anharmonicity. Further investigationsare required for a full understanding of this important and intricate topic.

* Electronic address: liquan777@calypso.cn
† Electronic address: mym@jlu.edu.cn
‡ Electronic address: chen@physics.unlv.edu

[1] G. Kresse and L. Furthmüller, Efficient Iterative Schemes for Ab initio Total-Energy Calculations Using a Plane-Wave Basis Set. Phys. Rev. B **54**, 11169 (1996).
[2] G. Kresse and D. Joubert, From Ultrasoft Pseudopotentials to the Projector Augmented-Wave Method. Phys. Rev. B **59**, 1758 (1999).
[3] D. M. Ceperley and B. J. Alder, Ground State of the Electron Gas by a Stochastic Method. Phys. Rev. Lett. **45**, 566 (1980).
[4] H. J. Monkhorst and J. D. Pack, Special Points for Brillouin-Zone Integrations. Phys. Rev. B **13**, 5188 (1976).
[5] J. Heyd, G. E. Scuseria, and M. Ernzerhof, Hybrid Functionals Based on a Screened Coulomb Potential. J. Chem. Phys. **118**, 8207 (2003).
[6] J. Heyd, G. E. Scuseria, and M. Ernzerhof, Erratum: Hybrid Functionals Based on a Screened Coulomb Potential. J. Chem. Phys. **124**, 219906 (2006).
[7] W. Bludau, A. Onton, and W. Heinke, Temperature dependence of the band gap of silicon, J. Appl. Phys. **45**, 1846 (1974).
[8] R. G. Humphreys, D. Bimberg, and W. J. Choyke, Wavelength modulated absorption in SiC, Solid State Commun. **39**, 163 (1981).
[9] Z. C. Pan, H. Sun, and C. F. Chen, Colossal shear-strength enhancement of lowdensity cubic BC_2N by nanoindentation. Phys. Rev. Lett. **98**, 135505 (2007).
[10] Z. C. Pan, H. Sun, Y. Zhang, and C. F. Chen, Harder than diamond: superior indentation strength of wurtzite BN and lonsdaleite. Phys. Rev. Lett. **102**, 1055503 (2009).
[11] B. Li, H. Sun, and C. F. Chen, Large indentation strain stiffening in nanotwinned cubic boron nitride. Nat. Commun. **5**, 4965 (2014).
[12] P. Giannozzi et al., QUANTUM ESPRESSO: a modular and open-source software project for quantum simulations of materials, J. Phys. Condens. Matter **21**, 395502 (2009).
[13] J. C. Thomas and A. Van der Ven, Finite-temperature properties of strongly anharmonic and mechanically unstable crystal phases from first principles, Phys. Rev. B **88**, 214111 (2013).
[14] F. Knoop, T. A. R. Purcell, M. Scheffler, and C. Carbogno, Anharmonicity measure for materials, Phys. Rev. Matter. **4**, 083809 (2020).
[15] H. Zhang, J. Tersoff, S. Xu1, H. Chen, Q. Zhang, K. Zhang, Y. Yang, C.-S. Lee, K.-N. Tu, J. Li, and Y. Lu, Approaching the ideal elastic strain limit in silicon nanowires, Sci. Adv. **2**, e1501382 (2016).
[16] A. Banerjee, D. Bernoulli, H. Zhang1, M. F. Yuen, J. Liu, J. Dong, F. Ding, J. Lu, M. Dao, W. Zhang, Y. Lu, S. Suresh, Ultralarge elastic deformation of nanoscale diamond, Science **360**, 300 (2018).
[17] A. Nie, Y. Bu, P. Li, Y. Zhang, T. Jin, J. Liu, Z. Su, Y. Wang, J. He, Z. Liu, H. Wang, Y. Tian, and W. Yang, Approaching diamond担theoretical elasticity and strength limits, Nat. Commun. **10**, 5533 (2019).
[18] M. Chen, L. Pethö, A. S. Sologubenko, H. Ma, J. Michler, R. Spolenak, and J. M. Wheeler, Achieving micron-scale plasticity and theoretical strength in Silicon, Nat. Commun. **11**, 2681 (2020).
[19] Z. Shi, M. Dao, E. Tsymbalov, A. Shapeev, J. Li, and S. Suresh, Metallization of diamond, Proc. Natl. Acad. Sci. (USA) **117**, 24634 (2020).
[20] C. Dang, J. Chou, B. Dai, C. Chou, Y. Yang, R. Fan, W. Lin, F. Meng, A. Hu, J. Zhu, J. Han, A. M. Minor, J. Li, Y.Lu, Achieving large uniform tensile elasticity in microfabricated diamond, Science **371**, 76 (2021).
[21] I. Errea, M. Calandra, C. J. Pickard, J. R. Nelson, R. J. Needs, Y. Li, H. Liu, Y. Zhang, Y. Ma, and F. Mauri, Quantum hydrogen-bond symmetrization in the superconducting hydrogen sulfide system, Nature **532**, 81 (2016).
[22] G. Shen, D. Ikuta, S. Sinogeikin, Q. Li, Y. Zhang, and C. F. Chen, Direct Observation of a Pressure-Induced Precursor Lattice in Silicon, Phys. Rev. Lett. **109**, 205503 (2012).